Dynamical nuclear decoupling of electron spins in molecular graphenoid radicals and biradicals

Federico Lombardi,[1,*] William K. Myers,[2] Ji Ma,[3] Junzhi Liu,[4] Xinliang Feng,[3] and Lapo Bogani[1,†]

[1]*Department of Materials, University of Oxford, 16 Parks Road, Oxford OX1 3PH, United Kingdom*
[2]*Inorganic Chemistry, University of Oxford, South Parks Road, Oxford OX1 3QR, United Kingdom*
[3]*Centre for Advanced Electronics, Faculty of Chemistry and Food Chemistry, Technische Universität, Monnsenstraße 4, 01069 Dresden, Germany*
[4]*Department of Chemistry and State Key Laboratory of Synthetic Chemistry, The University of Hong Kong, Pokfulam Road, Hong Kong, China*

We investigate the mechanisms of nuclear decoupling in synthetically tailored graphenoids, where the electron spin state is introduced by topological manipulation of the lattice. We compare molecular graphenoids containing one and two spin centers, introduced by pentagonal rings in the honeycomb lattice. Exploiting the molecular nature of the systems, we investigate the role of different nuclear species and environments. Variations on the Carr-Purcell-Meiboom-Gill pulse trains are used to prolong the coherence time of the electron spin of the radicaloids, leading to substantial improvements in performance and coherence times up to 300 μs at liquid-nitrogen temperature. The investigation of electron spin coherence as a function of interpulse spacing, with times close to the inverse of the nuclear precession frequency, reveals that a train of pulses in phase with the nuclear precession maximizes the nuclear decoupling. At room temperature the limits imposed by the sample treatment and environment are reached, indicating what amelioration is necessary to further enhance the quantum performance.

I. INTRODUCTION

It is of paramount importance, for quantum applications, that the coherence time of a superposition of states is long enough to enable gate operations with sufficient fidelity [1]. As a consequence the decoherence mechanisms of quantum systems and ways to prevent them are currently under intense scrutiny [2].

Solid-state spin quantum bits usually carry with them the presence of a nuclear environment [3]. How well this environment is defined, and whether it can actually be used to store and retrieve information, depends on the specific system under investigation. In some instances the nuclear environment can be a major source of decoherence, and where structural indetermination is present, this may produce considerable issues in the operation and standardization of the quantum bits. As a consequence, much attention is currently paid to ways of decoupling the nuclear spin bath from the electronic one [4–7] or, conversely, to the opportunities that can lie in carefully exploiting the nuclei-electron spin interactions [8–10]. These two seemingly different approaches are actually technically intimately connected: they both involve controlling the hyperfine coupling with an external train of impulses which will have the effect of polarizing the nuclear spins and projecting their state onto the electron spin, which is then measured [11].

The investigation of defects in solids has proved to be very fertile ground for quantum materials, and impressive quantum properties have been recorded in nitrogen-vacancy (NV) centers in diamond [12] and in color centers in silicon

carbide (SiC) [13]. Molecular systems have also produced increased enthusiasm in the past few years for their possible applications in the nanoregion and the almost infinite tunability offered by synthetic chemistry in terms of tailoring magnetic [14–16], optical [17], and electrical [18] properties of molecular groups. While, initially, it was thought that the quantum properties of molecular systems might be hampered by short coherence times [19], careful materials design using nuclear spin free ligands [20,21] and exploitation of clock transitions [22–24] brought molecular systems as stable protagonists onto the horizon of qubits candidates [25,26].

Carbon nanomaterials are particularly interesting in this regard because of their conducting and mechanical properties, the very low spin-orbit coupling [27], the presence of edge states [28], and topologically engineered states [29]. Although carbon nanotubes have shown low coherence times [30], of the order of nanoseconds at millikelvin temperature T, we recently reported microsecond coherence in synthetically tailored graphenoids, where pentagonal defects can be introduced at precise positions [31]. These systems allow studying the effects of topology on the quantum properties of graphene, as pentagonal sites introduce a spin triplet component into the electronic wave function. Superior quantum coherence at nitrogen T is obtained, and up to 2-μs coherence time in solution is reached at room T.

One way of overcoming the issue of nuclei-induced decoherence is to engineer the material using isotopic enrichment, cutting down the fraction of spin-containing nuclei [32]. It is anyway desirable to develop new methods to prolong the electron spin coherence without having to introduce ultra-pure environments: not only does this eliminate a difficult and expensive material engineering step, but it may also widen the

─────────
*federico.lombardi@materials.ox.ac.uk
†lapo.bogani@materials.ox.ac.uk

(a) Monoradical (2%)   Biradical
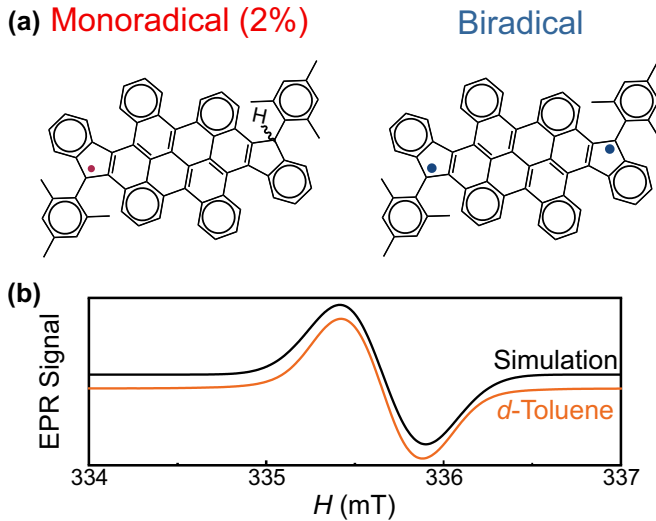

(b)

FIG. 1. (a) Chemical structure of the monoradical (left) and the biradical (right) graphenoids studied here. Hydrogen atoms are omitted, except for the one that is responsible for the different mono- and biradical characters owing to incomplete dehydrogenation. (b) Continuous-wave EPR signal measured at room temperature at 9.40 GHz for a *d*-toluene solution (orange) and simulation with the Hamiltonian in Eq. (1) (black).

range of environments where the quantum center can be operated. To this aim nucleus-electron spin-spin decoupling can be employed [4], e.g., by using the Carr-Purcell-Meiboom-Gill (CPMG) sequence of pulses [33,34]. CPMG was originally developed for structural nuclear magnetic resonance studies, but its applicability to the enhancement of quantum units is recognized.

Here we detail the effect of CPMG pulse sequences on the electron spin coherence of molecularly made graphenoids in frozen solutions at 100 K. We briefly introduce the quantum system; we explore its unoptimized coherence time and then proceed to enhance it with dynamical decoupling. We show that we can selectively decouple a specific nucleus by tailoring the time interval between pulses in a CPMG sequence, and we discuss the limits and advantages of this approach.

II. EXPERIMENTS AND ANALYSIS

The graphenoids explored in this study are produced with a bottom-up approach [31]. Using an organic synthetic approach [35–39], it is possible to create aromatic molecular systems that contain 16 hexagonal rings and 2 pentagonal rings placed with atomic precision to create an available open-shell ground state in each molecule and spin-bearing centers, as depicted in Fig. 1(a). The resulting molecular graphenoids contain one or more spin centers, depending on the hydrogenation of the rings. Monoradical and biradical molecular species are sometimes mixed in the compounds, with a molar fraction of monoradicals of $\simeq 0.02$ [31].

The spin properties of the system are described by the following Hamiltonian [31]:

$$\mathcal{H}_0 = \mu_B(S_1 + S_2)gH + S_1 J S_2 + \sum_{j=1}^{N} S A_j I_j, \quad (1)$$

where H is the external magnetic field, μ_B is the Bohr magneton, g is the electron Landé factor, J is the exchange interaction between the electronic spins S_1 and S_2, the A_j parameters describe the hyperfine interaction with the nuclear spins I_j, and the sum runs over all N interacting nuclei (both intra- and intermolecular ones, including carbon, hydrogen, and deuterium atoms). As previously reported [31], the exchange interaction $J \sim -550$ K, and the molecules are in an antiferromagnetic ground state, with a closely lying ferromagnetic excited state that can be populated by increasing T. Because the biradical is coupled antiferromagnetically and the monoradical is present in a fraction of a few percent, the monoradical species dominates the magnetic signal at $T \leqslant 80$ K. These monoradical molecules can be modeled using the same Hamiltonian in Eq. (1), simply ignoring one of the electron spins. As previously reported [31], the molecular fraction $\alpha \sim 2\%$ is estimated from the T dependence of the electron paramagnetic resonance (EPR) signal and magnetization measurements.

The samples were tested by preparing three solutions with a concentration of 1.5 ± 0.5 mM: in toluene, deuterated toluene (*d*-toluene), and carbon disulfide (CS$_2$). These three solvents offer platforms with different hyperfine baths: toluene contains eight hydrogen atoms and seven carbon atoms with the natural concentration of ^{13}C; deuteration decreases the hyperfine contribution of hydrogen atoms, substituting them with weaker deuterium. Eventually, CS$_2$ contains only the natural percentage of ^{13}C. In this way the effect of nuclei both in the environment and inside the molecule itself can be probed.

We measure the coherence times in ensembles through pulse EPR [40]. In EPR experiments the spin levels are split by the application of the static magnetic field H, and the spin transitions are excited using microwave irradiation inside a microwave resonator of relatively low quality factor $Q \simeq 300$. In the following we exclusively operate at the X band, i.e., at 9.40 GHz. We carried out the experiments in a Bruker Elexsys E580 equipped with a 1-kW traveling wave tube amplifier and a Bruker ER4118X-MS-3W1 resonator. T was regulated by an Oxford Instruments CF9350 cryostat with ITC503. Simulation of the static EPR spectra was performed using Eq. (1) and the MATLAB package EASYSPIN [41]. Good agreement is obtained with $g = 2.0027 \pm 0.0005$, while A_j were not resolved in this type of measurement [Fig. 1(b)].

The evolution of the spin wave function contains a part that sees momentum exchange with the lattice (i.e., will produce variations of the S_z component of the spin) and a part that produces only a variation in the phase of the wave function, i.e., that contains most of the quantum information. This quantum evolution of a spin is often visualized as a movement over the Bloch sphere, as in Fig. 2: zenith positions indicate pure $|\uparrow\rangle$ and $|\downarrow\rangle$ states, and any possible quantum state $|\psi\rangle = \cos\theta/2|\uparrow\rangle + e^{i\phi}\sin\theta/2|\downarrow\rangle$ is represented by a point on the spherical surface. The decay times of the two parts are defined as T_1 (representing vertical displacement on the Bloch sphere or variations of θ) and T_2 (evolution of the quantum phase ϕ, described by the azimuthal movement), which are also called spin-lattice and coherence times, respectively. In the literature several notations and definitions of the coherence time can be retrieved. Here we refer to the coherence time as
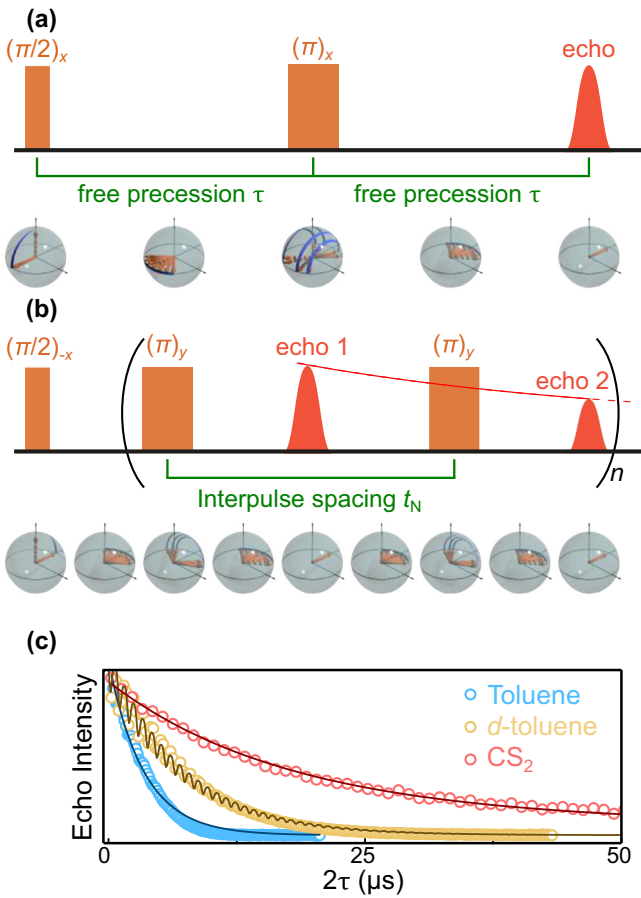
FIG. 2. (a) Pulse sequence used for the detection of the Hahn echo and effect of the pulses on the Bloch sphere. (b) Pulse sequence used for the detection of coherence with decoupling from the nuclear bath by CPMG. (c) Decay of the Hahn echo signal, as recorded in different solvents: toluene (blue), deuterated toluene (yellow), and CS_2 (red). Lines are fits to the data with Eq. (2). All measurements are performed at 9.40 GHz and $T = 100$ K.

T_m, and by this we consider a time which encompasses the contribution of T_2 and other effects such as instantaneous and spectral diffusion, residual dipolar interactions in dilution, and orientational averaging [40], so that, in general, $T_m \leqslant T_2$.

Measurements that fully include the effect of the nuclear bath, i.e., without any attempt at nuclei-electron spin decoupling, are acquired using a Hahn echo sequence [Fig. 2(a)]. The experiment is performed by using a microwave $\pi/2$ pulse resonant with the spin transitions applied along the x axis of the rotating frame. In this way the molecular spin state is transformed into the superposition state $|\Psi\rangle = (|\uparrow\rangle + |\downarrow\rangle)/\sqrt{2}$. To better describe the effect of the pulses we can use the propagator formalism. During the pulse the total Hamiltonian of the system is $\mathcal{H} = \mathcal{H}_0 + \omega_1 S_x$, and the evolution operator can be written as $U = \exp -i \int \mathcal{H} dt$. In the free precession the Hamiltonian is only $\mathcal{H}_0$ with propagator operator $U = e^{i\mathcal{H}_0 t}$. This means that when brought in the xy plane the different spin packets having different resonance frequencies ω_i will accumulate a phase difference $\Delta\phi = (\omega_i - \omega_{mw})\tau$. The phases are then refocused by the π pulse and are detected as an echo. The decay of the echo signal on changing the free

precession time is depicted in Fig. 2(c) for all the solvents. We fit the decay of echo signal $Y(t)$ as a function of time t with

$$Y(t) = Y_0 \left[\xi_1 \exp\left(\frac{-t}{T_m^{mono}}\right) + \xi_2 \exp\left(\frac{-t}{T_m^{bi}}\right) \right] \Xi(t), \quad (2)$$

where the coherence times of the monoradical and biradical species are labeled T_m^{mono} and T_m^{bi} and the coefficients ξ_i are their respective weights.

$\Xi(t) = 1 + [k_1 \sin(2\omega\tau + \phi_1) + k_2 \sin(4\omega\tau + \phi_2)]$ introduces a signal modulation given by the hyperfine coupling at a nucleus-specific frequency. The frequency of the nuclear precession is the Larmor frequency $\omega = \gamma_i H$, where γ_i is the gyromagnetic ratio of the specific nucleus. Given the excitation frequency used and considering that it can vary slightly in the setup of one experiment to another, we obtain the resonant field: $H \sim 340$–350 mT. This field corresponds to Larmor frequencies $\omega/2\pi = 14.8$ MHz for ^{1}H and 2.4 MHz for ^{2}H, with amplitudes k_1 and k_2 and phases ϕ_1 and ϕ_2 for first- and second-order effects. Because the frequency is nuclear specific, it can actually be used as a fingerprint of the dominant nuclear effects, but in the Hahn echo fitting procedure, the Ξ term does not directly change the extraction of the $T_m^{(i)}$. Hyperfine interactions are responsible for part of the decoherence, but for the purposes of fitting the echo decay signal and extracting $T_m^{(i)}$, the nuclear modulation and the electron spin coherence decay act as two distinct parts of the fitting function: the $T_m^{(i)}$ free parameters are independent of Ξ, and Ξ provides only information on the nuclear species that are creating signal oscillations.

The weights ξ_i in Eq. (2) are determined by the singlet-triplet energy splitting $|J| = 550$ K and the monoradical molecular fraction $\alpha \sim 2\%$:

$$\xi_2 = \frac{e^{-J/k_B T}}{\alpha + e^{-J/k_B T}}, \quad \xi_1 = 1 - \xi_2. \quad (3)$$

Error analysis shows that the largest error contribution arises from uncertainties in the values of ξ_i. We considered a variation of $\pm 20\%$ in the value of ξ_2 and fitted the experimental traces with the three pairs of ξ_i obtained. We then extrapolated the error as the maximum difference between the two extreme values of ξ_i and the central values. For all the solvents, we found that a 20% variation of ξ_2 produced about the same error on T_m^{bi}, and this quantity was plotted as error bars.

The nuclear modulation of the decay is visibly different, with different ω for the three solvents. The k_1 and k_2 are usually very small for hydrogen, and the modulation can be seen only for high sampling frequency, which, conversely, is not ideal if you want to observe a long decay; therefore, modulation effects are not well represented in Fig. 2(c) for toluene. On the other hand, modulation is very clear for the deuterium in d-toluene, which has large modulation depth k_1 and k_2 and low frequency. In the case of d-toluene we could expect to observe the effect of the intramolecular hydrogens; however, their modulation is completely overshadowed by the deuterium and cannot be resolved in this type of measurement despite the two contributions being at two different frequencies. Similarly, for CS_2 no modulation is observed because the solvent gives no nuclear contribution and the intramolecular hydrogens are too weak to produce a modulation in this type of measurement.

Having observed that nuclear modulation of the decay is an important factor in the Hahn echo, we now investigate dynamical decoupling as a way to increase robustness of electron coherence against nuclear hyperfine noise. Multiple schemes have been suggested [33,34,42–45], e.g., periodic and concatenated dynamical decoupling. In periodic dynamical decoupling the train of pulses is spaced at the same interval, and the CPMG decoupling scheme belongs to this family [Fig. 2(b)]. In concatenated dynamical decoupling, the pulses are optimized to be at a specific time, and the interpulse spacing is different between adjacent decoupling pulses: Uhrig dynamical decoupling (UDD) is one example [44]. The theory predicts that in the case of an environmental bath with a hard-cutoff spectral density [3], UDD performs better than CPMG, while in the presence of a soft cutoff they have comparable efficiency [46]. However, it is often hard to make theoretical predictions without a specific reference to a quantum system, and CPMG outperforms UDD when the bath is composed of weakly coupled nuclei [47,48].

We employed a two-step phase cycling on the initial pulse to eliminate pulse offset effects [40,48]. Each CPMG measurement produced a set of echoes; the maximum of each echo was fitted with the model in Eq. (2), where no modulation is expected [as depicted in Fig. 2(b)]. The trend of the signal can then be followed on varying the interpulse spacing t_N between the π pulses of the CPMG train [Fig. 2(b)]: for each t_N value one decay trace is obtained, from which we extract the two decay constants T_{CPMG}^{mono} and T_{CPMG}^{bi} for the monoradical and biradical species, respectively. We compare the results with the precession periods of the nuclei involved: hydrogen, deuterium, and carbon. The precession period is just the inverse of the Larmor frequency, and under our experimental conditions we obtain $T_H \simeq 70$ ns, $T_D \simeq 457$ ns, and $T_C \simeq 280$ ns (for ^{13}C).

Figure 3 displays the resulting behavior of the $T_{CPMG}^{(i)}$ when varying the interpulse spacing in toluene. The signal is mainly modulated by the precession of the ^{1}H nuclei, and decays rapidly on increasing the interpulse spacing as predicted by theory [49]. This is to be assigned to both intra- and intermolecular ^{1}H atoms, as the toluene solvent molecules are capable of π stacking onto the aromatic surface of the graphenoids. In Fig. 3 it is also clear how the efficiency of the decoupling technique decreases when increasing the interpulse spacing. If the spacing is large, the spins are allowed to decohere between one pulse and the next one, and the effect of the decoupling becomes less evident. Ultimately, how fast this happens depends on the unoptimized value of T_m measured through the Hahn echo sequence: when the interpulse spacing $t_N \simeq T_m$, the CPMG decoupling will not be effective.

The maximum decoupling is obtained when the interpulse spacing is equal to an integer multiple of the precession period of the targeted nucleus. In other words, if the train of refocusing pulses is perfectly in phase with the precession of the nuclei, the quantum phase becomes more robust against the decohering effect of the nuclei themselves. For both mono- and biradicals $T_{CPMG}^{(i)}$ can reach, in the in-phase scenario, up to 5 times larger than if the pulse sequence is out of phase with the nuclear precession.

The behavior in *d*-toluene, shown in Fig. 4, displays $T_{CPMG}^{(i)}$ modulated by both by the ^{1}H and ^{2}H nuclei. Here it is
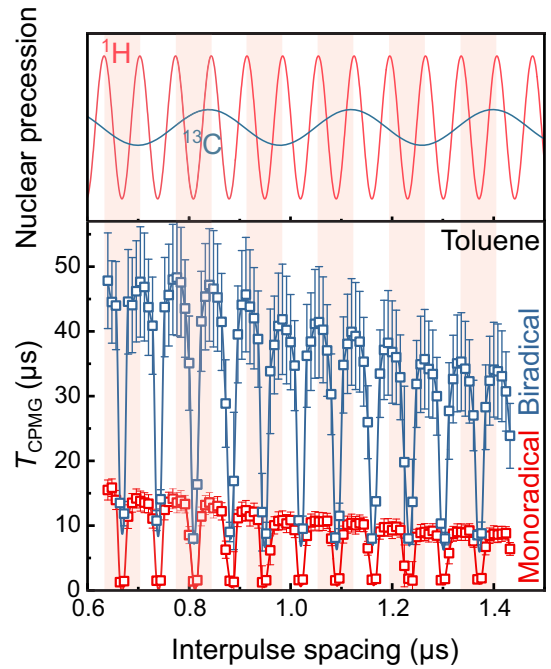

FIG. 3. Top: Periodic oscillations of the nuclear signal of an ensemble, as produced by precession, for ^{1}H hydrogen (red) and ^{13}C (blue) atoms. Bottom: experimental dependence of the decay time T_{CPMG} as a function of the interpulse spacing interval t_N. The signals for the monoradical and biradical species are plotted in red and blue, respectively. In both panels the periodicity of the hydrogen nuclei is highlighted by red shading. All measurements were acquired in toluene at $T = 100$ K.

relevant to highlight the effect of the ^{1}H nuclei. Indeed, above we stated that their modulation was not detected in the simple Hahn echo experiment. However, when using CPMG, the effect is distinguishable, and the modulation depth is analogous to the one produced by the ^{2}H nuclei. This result needs to be included in a wider picture that encompasses the possibility of detecting very weakly coupled nuclei with dynamical decoupling techniques. This was proved in the literature in the case of NV centers [11]. And in this case a careful understanding of the dynamics of the decoupling could pave the way to electron to nuclear coherence transfer and storing of the quantum phase on the nuclear coherence.

Finally, in Fig. 5 we note that in CS_2 hydrogens are again the main modulating factor. Like in the *d*-toluene case, a very strong modulation now appears which is a fingerprint of very weakly coupled intermolecular hydrogens. Significantly, T_{CPMG}^{bi} initially increases when increasing the interpulse spacing, contrary to the behavior in toluene and *d*-toluene. However, if we track $T_{CPMG}^{(i)}$ for long t_N up to 14 μs (Fig. 5, right panel), we find again the decay that we attributed to the efficiency of the decoupling sequence. We explain the initial rise considering that the decay time observed in CS_2 is much larger than $T_{CPMG}^{(i)}$ in the other solvents, and accordingly, the number of pulses required to map it is also considerably larger: up to 400 pulses are required. In this case, imperfections in the pulse shaping should also be considered: there is a systematic error in pulse formation that accumulates when in the presence of many pulses [50]. Pulse errors can thus
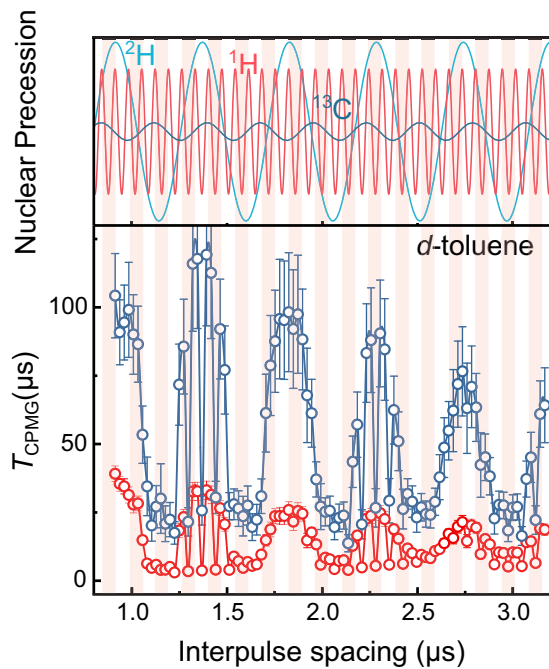
FIG. 4. Top: Periodic oscillations of the nuclear signal of an ensemble, as produced by precession, for ^{2}D deuterium (teal), ^{1}H hydrogen (red), and ^{13}C (blue) atoms. Bottom: experimental dependence of the decay time T_{CPMG} as a function of the interpulse spacing interval t_{N}. The signals for the monoradical and biradical species are plotted in red and blue, respectively. In both panels the periodicity of the hydrogen nuclei is highlighted by red shading. All measurements were acquired in deuterated toluene at $T = 100$ K.

FIG. 5. Left: Periodic oscillations of the nuclear signal of an ensemble, as produced by precession, for ^{1}H hydrogen (red) and ^{13}C (blue) atoms and experimental dependence of the decay time T_{CPMG} as a function of the interpulse spacing interval t_{N}. The signals for the monoradical and biradical species are plotted in red and blue, respectively. The periodicity of the hydrogen nuclei is highlighted by red shading. All measurements were acquired in carbon disulfide at $T = 100$ K. Right: $T_{\mathrm{CPMG}}^{\mathrm{bi}}$ decay versus t_{N}; for simplicity only the maximum peaks over a period are shown, and error bars are removed.

become the main source of decoherence, limiting the benefits of a dynamical decoupling approach [51].

We evaluate the overall performance of the dynamical decoupling scheme in Fig. 6 by plotting together the Hahn echo decays, the CPMG traces for the three solvents, and the T_1 time, which is an upper limit to the coherence. Only T_1 measured in d-toluene is depicted because the spin-lattice relaxation time is independent of hyperfine coupling and produces a similar result in all three solvents. When the CPMG traces are compared to the respective Hahn echo coherence times and using the best interpulse spacing, we observe a more than tenfold increase by decoupling in toluene, a sixfold increase in d-toluene, and a threefold increase in CS_2. The most important relative improvement is obtained in toluene because it has the largest number of environmental nuclei, while the smallest improvement is obtained in the system with the best performance, CS_2, where very few environmental nuclei matter. In CS_2 we reach a coherence time of 0.3 ms, against a T_1 of 2 ms, while the maximum value attainable in theory would be $2T_1$. This theoretical limit is not reached because the decoupling can only mitigate the effect of the nuclei and cannot erase it completely. Were this the case, the coherence time in toluene after CPMG should also be the same as CS_2 without CPMG.

We wish to stress an often-overlooked aspect of dynamical decoupling: the presence of additional signals that arise when having multiple pulses. In EPR, for any three-pulse sequence, one should always observe a stimulated echo [40]. If the
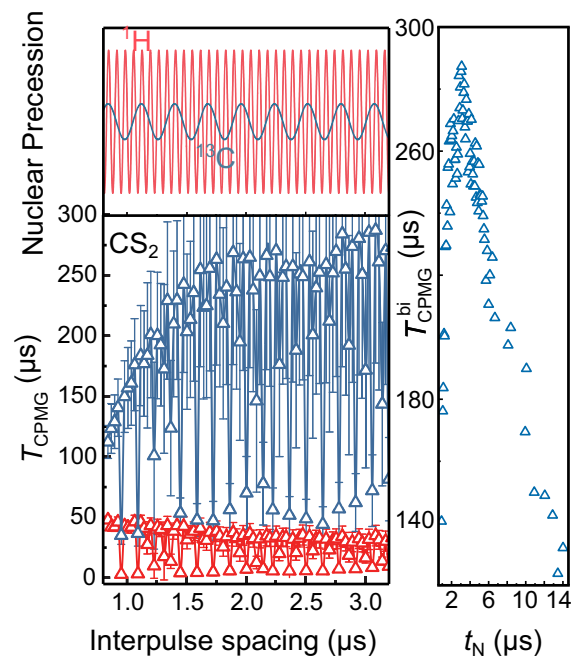
time distance between the pulses is the same, as in periodic dynamical decoupling, it is possible that the stimulated echo overlaps with the original echo signal, distorting the signal shape [Fig. 7(a)] and possibly mixing the T_{m} and T_1 times. In the sequence i Fig. 2 we used a two-step phase cycling: the first step has the $\pi/2$ pulse with a phase of 180°, and the second step has a phase of 0°, so that all π pulses are applied on the y axis, and their relative phase is always kept constant. In the context of the analysis of quantum systems, this choice is justified by the fact that the resulting time is still the time in which the quantum bit system can be operated meaningfully; that is, it corresponds to the desired quantity. On the other hand, it is instructive to understand how the overlap is affecting the results by using different phase cycling techniques that minimize it. To completely eliminate unwanted signals we would need a phase cycling with 4^{n-1} steps, where n is the number of π pulses [52], which would mean an absurdly large pulse sequence in the present case. We thus test the difference between the simple two-phase step cycling and a more complex scheme employing eight phases, as depicted in Fig. 7(b). In this more sophisticated phase cycling we still cycle the first $\pi/2$ pulse, but we also vary the phase difference among the following eight $(\pi)_y$ pulses. In Fig. 7(a) we define φ_i as the phase difference between two adjacent $(\pi)_y$ pulses. In each step of the scheme φ_i can assume a value 0° or 180°, which implies having $(\pi)_y$ or $(\pi)_{-y}$. In order to cancel the overlap of the signals the sequence is
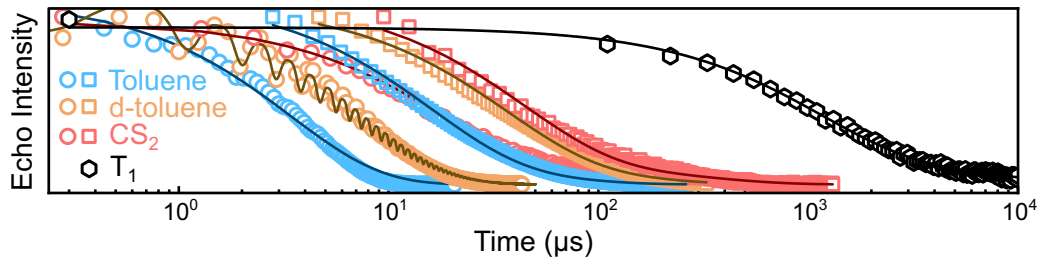
FIG. 6. Echo signal intensity as a function of the distance between the echoes and the first impulse $\pi/2$ for the Hahn echo (circles) and CPMG sequence (squares). Measurements are performed in toluene (turquoise), d-toluene (amber), and carbon disulfide (magenta). The spin-lattice relaxation time T_1 is also reported (black hexagons) as measured via a signal inversion recovery procedure, here displayed as a decay for simplicity. All measurements are performed at 9.40 GHz and $T = 100$ K.

cycled over all 2×2^7 possible different combinations, for a total of 256 steps.

The two approaches were tested at room temperature. In Fig. 7(c) we display the difference in the decay of the signal when the two different cycling sequences are employed. A discrepancy in the decay is clearly visible, with the 256-step measurement relaxing faster than the two-step one. Additionally, in the 256-step measurement all eight echoes assume
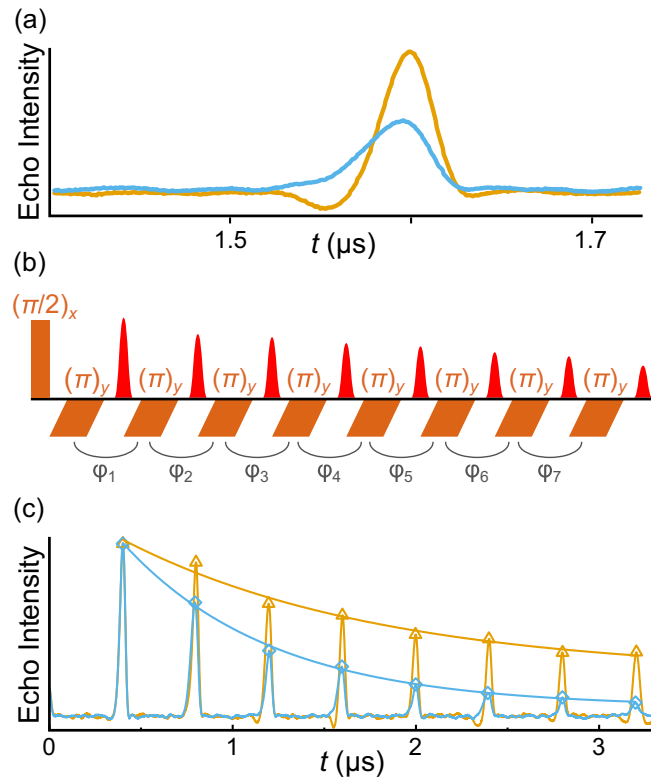

FIG. 7. (a) Distortion of the echo signal produced by the overlap of multiple echoes in the two-step phase cycling of the CPMG sequence (orange). The equivalent echo signal after eight-phase cycling is also depicted (blue). (b) Pulse sequence for eight-phase cycling in CPMG: after the initial $\pi/2$ step, the next eight π_y pulses have a φ_i phase that cyclically assumes a value $0°$ or $180°$. (c) Comparison of the echo decays obtained in CPMG with two-step phase cycling and the 256-step one. Black lines are single exponential fits of the maximum of the echoes. All measurements are performed at room temperature.

an almost ideal shape [Fig. 7(a)], while the stimulated echo distorts the shape of the higher-order echoes in the two-step phase cycling.

The variation of the results between the two different phase cyclings can be attributed, once again, to pulse formation errors. The π pulses in the train are supposed to refocus the phase of the different spin packets by rotating them in the xy plane. That is what is depicted in the Bloch sphere representation in Fig. 2. However, because the rotation angle of a pulse is subjected to errors, the spin packets can be brought outside of the xy plane, thus gaining a small but non-negligible z component. Using a scheme that cycles the train of π pulses between y and $-y$ compensates for pulse formation errors and mitigates the formation of a vertical displacement. When discussing the time decay T_{CPMG} for standard two-step phase cycling, it is useful to point out that this might contain an admixture of T_m and T_1 because the vertical displacement decays following T_1.

III. CONCLUSIONS

In conclusion, our measurements show in detail how CPMG sequences can be used to enhance the coherence time of molecular graphenoids and how the sequences can be tailored depending on the specific environment of the molecules to optimize their quantum performance. The main source of decoherence in frozen solutions in the temperature range 80–150 K comes from the hyperfine contribution of the nuclei in the solvent and in the molecules: hydrogen and carbon atoms. The investigation of the effect of solvents highlights the important role played by the environment and the possibility of increasing the coherence times by addressing nuclei contained in the solvent molecules, instead of the molecular ones. The inclusion in environments that have a very low content of active nuclei, thus reducing the solvent nuclear bath, allowed decoupling selectively from the molecular hydrogens. We determine that the hydrogens are the nuclei contributing the most to the decoherence, and indeed, their modulation can be clearly seen independently of the solvent. Therefore, isotopic substitution of the hydrogens in the molecules could produce a significant increase of the coherence time. In fact, even when maximally decoupled, the coherence time in toluene is still half the one of decoupled d-toluene. On the other hand, there is no strong evidence of modulation of ^{13}C even in CS_2. Due to the very low abundance of the isotope we are unable to

detect its effect, although it could become more relevant in planned single-molecule measurements.

In addition we have explored possible sources of errors, with particular attention to the possibility of residual T_1 components in T_{CPMG}. While such tests are important on the methodological level, it is fundamental to stress that, while achieving a 2^n step phase cycling for 8 pulses is possible, it becomes more challenging when increasing the number of pulses, and already for 20 pulses the scheme would require 10^6, which is technologically infeasible.

On a different note, our results indicate that the coherence time could still be improved upon by technical improvement in the experimental setup. First of all, a larger bandwidth resonator would allow minimizing the interpulse spacing to the time of a single revolution of hydrogens, which under this condition we found to be $T_H \simeq 70$ ns. Second, to make up for the large number of pulses required, a possible perspective is to implement additional correction schemes. One option is to introduce and compare other decoupling sequences, such as those tested for other quantum units [45,47,53–59]. Another possible source of inspiration arises from the efforts to correct pulse formation errors produced in nuclear magnetic resonance, albeit for different instrumentation, and whether they can be adapted to EPR in this particular situation. In theory, it would be possible to reduce the errors either using composite pulses [60–62] or shaped pulses [63]. Careful studies will regardless need to consider that the use of advanced pulse techniques comes at the expense, in both cases, of an increase in the pulse duration time and therefore slower spin manipulation. Additionally, it would be possible to use so-called self-correcting sequences. These are dynamical decoupling sequences that employ rotations around multiple axes and are expected to correct pulse formation errors. One example is the XY4 sequence that was developed for NMR as an upgrade of CPMG [64]. This scheme has seen interesting theoretical developments in the past few years and experimental proof of better performances than CPMG [45,47,58,59]. Future studies of dynamical decoupling in molecular systems should incorporate the XY paradigm.

At room temperature the resulting decoherence is no longer dominated by the nuclear bath, as the limit of $T_m \simeq 2T_1$ is reached. Any attempt of CPMG at this regime did not yield any improvement in the coherence time. This indicates rational synthetic routes that can be used to improve the room-T coherence or integration into devices, e.g., via imprisonment into matrices such as zeolites and porous membranes or into liquid crystals. These results also open the path to the use of disperse graphenoids for sensing applications [65] in various environments [66–68], and applications in biosciences and nanotechnology seem particularly interesting, also considering the hydrophobic and amphiphilic properties of biological membranes.

[1] M. A. Nielsen and I. Chuang, *Quantum Computation and Quantum Information* (Cambridge University Press, 2011).

[2] T. D. Ladd, F. Jelezko, R. Laflamme, Y. Nakamura, C. Monroe, and J. L. O'Brien, Nature (London) **464**, 45 (2010).

[3] N. V. Prokof'ev and P. C. E. Stamp, Rep. Prog. Phys. **63**, 669 (2000).

[4] L. Viola, E. Knill, and S. Lloyd, Phys. Rev. Lett. **82**, 2417 (1999).

[5] H. Bluhm, S. Foletti, I. Neder, M. Rudner, D. Mahalu, V. Umansky, and A. Yacoby, Nat. Phys. **7**, 109 (2011).

[6] T. Van Der Sar, Z. H. Wang, M. S. Blok, H. Bernien, T. H. Taminiau, D. M. Toyli, D. A. Lidar, D. D. Awschalom, R. Hanson, and V. V. Dobrovitski, Nature (London) **484**, 82 (2012).

[7] N. Bar-Gill, L. M. Pham, C. Belthangady, D. Le Sage, P. Cappellaro, J. R. Maze, M. D. Lukin, A. Yacoby, and R. Walsworth, Nat. Commun. **3**, 858 (2012).

[8] H. S. Knowles, D. M. Kara, and M. Atatüre, Phys. Rev. B **96**, 115206 (2017).

[9] M. H. Abobeih, J. Cramer, M. A. Bakker, N. Kalb, M. Markham, D. J. Twitchen, and T. H. Taminiau, Nat. Commun. **9**, 1 (2018).

[10] C. E. Bradley, J. Randall, M. H. Abobeih, R. C. Berrevoets, M. J. Degen, M. A. Bakker, M. Markham, D. J. Twitchen, and T. H. Taminiau, Phys. Rev. X **9**, 031045 (2019).

[11] G.-Q. Liu, J. Xing, W.-L. Ma, P. Wang, C.-H. Li, H. C. Po, Y.-R. Zhang, H. Fan, R.-B. Liu, and X.-Y. Pan, Phys. Rev. Lett. **118**, 150504 (2017).

[12] M. Atatüre, D. Englund, N. Vamivakas, S. Y. Lee, and J. Wrachtrup, Nat. Rev. Mater. **3**, 38 (2018).

[13] D. D. Awschalom, R. Hanson, J. Wrachtrup, and B. B. Zhou, Nat. Photonics **12**, 516 (2018).

[14] L. Bogani, J. Appl. Phys. **109**, 07B115 (2011).

[15] S. Jiang, K. Goß, C. Cervetti, and L. Bogani, Sci. China Chem. **55**, 867 (2012).

[16] S.-D. Jiang, D. Maganas, N. Levesanos, E. Ferentinos, S. Haas, K. Thirunavukkuarasu, J. Krzystek, M. Dressel, L. Bogani, F. Neese *et al.*, J. Am. Chem. Soc. **137**, 12923 (2015).

[17] R. Moroni, R. Buzio, A. Chincarini, U. Valbusa, F. B. de Mongeot, L. Bogani, A. Caneschi, R. Sessoli, L. Cavigli, and M. Gurioli, J. Mater. Chem. **18**, 109 (2008).

[18] R. Chen, R.-Q. Lu, P.-C. Shi, and X.-Y. Cao, Chin. Chem. Lett. **27**, 1175 (2016).

[19] A. Ardavan, O. Rival, J. J. L. Morton, S. J. Blundell, A. M. Tyryshkin, G. A. Timco, and R. E. P. Winpenny, Phys. Rev. Lett. **98**, 057201 (2007).

[20] J. M. Zadrozny, J. Niklas, O. G. Poluektov, and D. E. Freedman, ACS Cent. Sci. **1**, 488 (2015).

[21] C.-J. Yu, M. J. Graham, J. M. Zadrozny, J. Niklas, M. D. Krzyaniak, M. R. Wasielewski, O. G. Poluektov,

and D. E. Freedman, J. Am. Chem. Soc. **138**, 14678 (2016).

[22] M. Shiddiq, D. Komijani, Y. Duan, A. Gaita-Ariño, E. Coronado, and S. Hill, Nature (London) **531**, 348 (2016).

[23] J. M. Zadrozny, A. T. Gallagher, T. D. Harris, and D. E. Freedman, J. Am. Chem. Soc. **139**, 7089 (2017).

[24] A. Gaita-Ariño, F. Luis, S. Hill, and E. Coronado, Nat. Chem. **11**, 301 (2019).

[25] J. M. Clemente-Juan, E. Coronado, and A. Gaita-Ariño, Chem. Soc. Rev. **41**, 7464 (2012).

[26] E. Coronado, Nat. Rev. Mater. **5**, 87 (2019).

[27] B. Trauzettel, D. V. Bulaev, D. Loss, and G. Burkard, Nat. Phys. **3**, 192 (2007).

[28] M. Slota, A. Keerthi, W. K. Myers, E. Tretyakov, M. Baumgarten, A. Ardavan, H. Sadeghi, C. J. Lambert, A. Narita, K. Müllen *et al.*, Nature (London) **557**, 691 (2018).

[29] S. Mishra, D. Beyer, K. Eimre, S. Kezilebieke, R. Berger, O. Gröning, C. A. Pignedoli, K. Müllen, P. Liljeroth, P. Ruffieux, X. Feng, and R. Fasel, Nat. Nanotechnol. **15**, 22 (2020).

[30] E. A. Laird, F. Pei, and L. P. Kouwenhoven, Nat. Nanotechnol. **8**, 565 (2013).

[31] F. Lombardi, A. Lodi, J. Ma, J. Liu, M. Slota, A. Narita, W. K. Myers, K. Müllen, X. Feng, and L. Bogani, Science **366**, 1107 (2019).

[32] G. Balasubramanian, P. Neumann, D. Twitchen, M. Markham, R. Kolesov, N. Mizuochi, J. Isoya, J. Achard, J. Beck, J. Tissler, V. Jacques, P. R. Hemmer, F. Jelezko, and J. Wrachtrup, Nat. Mater. **8**, 383 (2009).

[33] H. Y. Carr and E. M. Purcell, Phys. Rev. **94**, 630 (1954).

[34] S. Meiboom and D. Gill, Rev. Sci. Instrum. **29**, 688 (1958).

[35] A. Narita, X.-Y. Wang, X. Feng, and K. Müllen, Chem. Soc. Rev. **44**, 6616 (2015).

[36] J. Ma, J. Liu, M. Baumgarten, Y. Fu, Y. Z. Tan, K. S. Schellhammer, F. Ortmann, G. Cuniberti, H. Komber, R. Berger, K. Müllen, and X. Feng, Angew. Chem., Int. Ed. **56**, 3280 (2017).

[37] Y. G. Tullimi, W. Zeng, X. Lu, and J. Wu, Chem. Commun. **54**, 2186 (2018).

[38] Y. Ni, T. Y. Gopalakrishna, H. Phan, T. S. Herng, S. Wu, Y. Han, J. Ding, and J. Wu, Angew. Chem., Int. Ed. **57**, 9697 (2018).

[39] C. Liu, Y. Ni, X. Lu, G. Li, and J. Wu, Acc. Chem. Res. **52**, 2309 (2019).

[40] A. Schweiger and G. Jeschke, *Principles of Pulse Electron Paramagnetic Resonance* (Oxford University Press, Oxford, 2001).

[41] S. Stoll and A. Schweiger, J. Magn. Reson. **178**, 42 (2006).

[42] K. Khodjasteh and D. A. Lidar, Phys. Rev. Lett. **95**, 180501 (2005).

[43] O. Kern and G. Alber, Phys. Rev. Lett. **95**, 250501 (2005).

[44] G. S. Uhrig, Phys. Rev. Lett. **98**, 100504 (2007).

[45] D. Farfurnik, A. Jarmola, L. M. Pham, Z. H. Wang, V. V. Dobrovitski, R. L. Walsworth, D. Budker, and N. Bar-Gill, Phys. Rev. B **92**, 060301(R) (2015).

[46] K. Khodjasteh and D. A. Lidar, Phys. Rev. A **75**, 062310 (2007).

[47] G. de Lange, Z. H. Wang, D. Riste, V. V. Dobrovitski, and R. Hanson, Science **330**, 60 (2010).

[48] N. Bar-Gill, L. M. Pham, A. Jarmola, D. Budker, and R. L. Walsworth, Nat. Commun. **4**, 1743 (2013).

[49] G. A. Álvarez, A. Ajoy, X. Peng, and D. Suter, Phys. Rev. A **82**, 042306 (2010).

[50] J. J. L. Morton, A. M. Tyryshkin, A. Ardavan, K. Porfyrakis, S. A. Lyon, and G. A. D. Briggs, Phys. Rev. A **71**, 012332 (2005).

[51] J. H. Shim, I. Niemeyer, J. Zhang, and D. Suter, Europhys. Lett. **99**, 40004 (2012).

[52] J. Soetbeer, M. Hülsmann, A. Godt, Y. Polyhach, and G. Jeschke, Phys. Chem. Chem. Phys. **20**, 1615 (2018).

[53] M. A. Ali Ahmed, G. A. Álvarez, and D. Suter, Phys. Rev. A **87**, 042309 (2013).

[54] Z.-H. Wang, G. de Lange, D. Ristè, R. Hanson, and V. V. Dobrovitski, Phys. Rev. B **85**, 155204 (2012).

[55] A. Dréau, P. Jamonneau, O. Gazzano, S. Kosen, J.-F. Roch, J. R. Maze, and V. Jacques, Phys. Rev. Lett. **113**, 137601 (2014).

[56] A. M. Souza, G. A. Álvarez, and D. Suter, Philos. Trans. R. Soc. A **370**, 4748 (2012).

[57] J. E. Lang, T. Madhavan, J.-P. Tetienne, D. A. Broadway, L. T. Hall, T. Teraji, T. S. Monteiro, A. Stacey, and L. C. L. Hollenberg, Phys. Rev. A **99**, 012110 (2019).

[58] A. M. Souza, G. A. Ávarez, and D. Suter, Phys. Rev. Lett. **106**, 240501 (2011).

[59] J. Zhang, A. M. Souza, F. D. Brandao, and D. Suter, Phys. Rev. Lett. **112**, 050502 (2014).

[60] M. H. Levitt, Prog. Nucl. Magn. Reson. Spectrosc. **18**, 61 (1986).

[61] H. K. Cummins, G. Llewellyn, and J. A. Jones, Phys. Rev. A **67**, 042308 (2003).

[62] J. J. L. Morton, A. M. Tyryshkin, A. Ardavan, K. Porfyrakis, S. A. Lyon, and G. A. D. Briggs, Phys. Rev. Lett. **95**, 200501 (2005).

[63] P. E. Spindler, P. Schöps, W. Kallies, S. J. Glaser, and T. F. Prisner, J. Magn. Reson. **280**, 30 (2017).

[64] A. A. Maudsley, J. Magn. Reson. (1969-1992) **69**, 488 (1986).

[65] D. Schmid-Lorch, T. Häberle, F. Reinhard, A. Zappe, M. Slota, L. Bogani, A. Finkler, and J. Wrachtrup, Nano Lett. **15**, 4942 (2015).

[66] R. Konnerth, C. Cervetti, A. Narita, X. Feng, K. Müllen, A. Hoyer, M. Burghard, K. Kern, M. Dressel, and L. Bogani, Nanoscale **7**, 12807 (2015).

[67] C. Cervetti, E. Heintze, and L. Bogani, Dalton Trans. **43**, 4220 (2014).

[68] M. Mergenthaler, J. Liu, J. J. Le Roy, N. Ares, A. L. Thompson, L. Bogani, F. Luis, S. J. Blundell, T. Lancaster, A. Ardavan *et al.*, Phys. Rev. Lett. **119**, 147701 (2017).